Intrinsically High Refractive Index Silicone Polymers Containing S and P Heteroatoms

Meiqi Yang[1, 2, 3],Qinxue Han [2], Yulin Ding[2,3], Junfeng Li[2,3,4], and Wenmu Li[2, 3,4]*

[1] College of Chemistry and Materials, Fujian Normal University, Fuzhou, Fujian, China

[2] Key Laboratory of Optoelectronic Materials Chemistry and Physics, Fujian Institute of Research on the Structure of Matter, Chinese Academy of Sciences, Fuzhou, Fujian, China

[3] Fujian College, University of Chinese Academy of Sciences, Fuzhou, Fujian, China

[4] University of Chinese Academy of Sciences

*Corresponding Email: liwm@fjirsm.ac.cn

Abstract

There is growing interested in high refractive index polymers due to their numerous applications in optical materials. In current work, we reported a facile strategy to improve the refractive index of the optical materials. The new asymmetric binary thiol dopants containing high molar refractive index heteroatoms (S and P) and large conjugated groups were successfully designed and synthesized. Using these additives, the high refractive index silicone polymers were developed from these dopants and vinyl silicones simply via the light-cured reaction. The effects of dopants' structure and content on the thermal and optical properties of cured silicone polymers were systematically investigated. The results show that the asymmetry structure of the dopants can not only effectively offset the accumulated trend of the large conjugated groups but also improve the refractive index of cured silicone polymers. Even with 5% dopant's loading, the refractive index of the SOV-5 increased from 1.5773 to 1.5803 without notably sacrificing its the light transmittance. The glass transition temperature of the cured silicone polymers decreases, even though their crosslink density increase with the growing of the dopants' loading.

Keywords: High refractive index polymers; Light-curing; Organic silicon; Thiol-ene reaction

Introduction

In recent years, the electronics industry has witnessed significant growth due to the development of new industries and advancements in packaging technology [1-5]. As a result, the silicone materials have become increasingly popular due to their exceptional performance characteristics[6,7]. The silicon atom in these materials is typically bonded to a combination of oxygen atoms and a simple organic component. Increasing the content of silicon-oxygen makes these materials more "inorganic", which contributes to the high thermal stability and durability. While increasing the silicon-organic content makes them more "organic" contributing to their unique surface characteristics, insulating and soluble characteristics. Silicone properties and forms are defined by the balance of these contributions. Attaching more complex organic groups to these basic structures enables "silicone-organic hybrids," providing an extraordinary range of properties and societal benefits[8-10].

However, to meet the new demands of the growing industry, the silicone materials must perform even better, and increasing the refractive index of the material is one of the critical aspects[11]. There are two general approaches for increasing the refractive index of polymers. One is the hybrid of highly refractive inorganic nanoparticles with organic polymer chains to form nanocomposites [12-17]. The other is introducing high molar refractive index functional groups into the polymer chain[18]. While nanocomposites have a high refractive index, the aggregation of nanoparticles can compromise

their stability and processability[19-21]. Intrinsic HRIPs, on the other hand, offer superior stability and processability, although their upper refractive index limit is typically lower than 1.8. Usually, intrinsic HRIP is used to increase the refractive index of polymers by introducing some functional groups with high molar refractive index into the polymer chain, such as aromatic groups[22, 23], halogen elements other than F[24-26], or heteroatoms such as sulfur[27-31], nitrogen[32], and phosphorus[33-36].

Thiol-ene photoaddition reactions are widely used as an effective method for preparing cross-linked polymer systems, particularly for intrinsic high refractive index organosilicon rubbers. This is because the polarized sulfur atom can be used as an intrinsic part of the polymer repeating unit to increase the refractive index. In this study, the dithiol chain extenders, which contain high molar refractive index heteroatoms (S and P) and large conjugated groups, designed and used to prepare liquid crosslinkers. The high refractive index silicone polymers were developed from these liquid crosslinkers and vinyl silicones simply via the light-cured reaction. The resulting polymers exhibit high refractive index, good optical transmittance, as well as excellent thermal properties. The addition of asymmetric structural compounds counters the tendency of phenyl crystallization, leading to further improvements in the polymer's optical transmittance properties. The study also investigated the effect of the content of dimeric sulfhydryl compounds on the properties of high refractive index silicone resins.

Experimental section

Materials.

6H-dibenz(C,E)(1,2)oxaphosphorin-6-oxide（DOPO）， 4-hydroxybenzaldehyde， 4-Hydroxy-3-Methylbenzaldehyde，1,4-Diazabicyclo[2.2.2]octane Triethylene Diamine（DABCO）， N,N-Dimethylthiocarbamoyl Chloride（DMTCC），Phenyl ether ， β-Mercaptoethanol ， p-Toluenesulfonic acid (p-TSA) ， trichloro(phenyl)silane ，dimethoxy(methyl)(vinyl)silane (MVDMS)， diphenylsilanediol（DPSD） and Barium hydroxide monohydrate were obtained from Adamas-beta®. Methanol, ethanol, methylene chloride, triethylamine, phenol, ethyl ether, and DMF were purchased from Sinopharm Chemical ReagentCo., Ltd. T. After distillation from magnesium, trichloro (phenyl)silane was used as the starting material. The triethylamine and DMF were distilled from calcium hydride before use. Ether was dried over activated molecular sieves.

Instrumentation.

The ^{1}H-NMR, ^{13}C-NMR and ^{31}P-NMR spectra were recorded with Bruker AVANCE III400 instrument. The ^{29}Si-NMR spectra recorded with JEOL 600YH instrument. The fourier transform infrared (FT-IR) spectroscopy was performed on Nicolet iS5 FTIR Spectrometer at room temperature. The RI of the curing compounds was measured by an Abbe refractometer (1WAJ by SHANGHAI JINGKE INDUSTRIAL CO., LTD) at 25℃. The Lambda950 UV-Visible Spectrophotometer (PERKINELMER) was used for transmittance measurement. The thermal aging tests of the encapsulants were carried out by evaluating the transmittance of the encapsulant films before and after heating at 150℃ for 48h. The shore durometer (LX-D-2, Sanliang) was used for measuring the shore D hardness. The thermogravimetric analysis (TGA) was performed under a nitrogen flow using STA449C (Netzsch) with a heating rate of 10℃/min from 30℃ to 800℃. The dynamic mechanical analysis (DMA) was performed using Q800 (TA instrument) with a ramp rate of 5℃/min at a constant frequency (1 Hz) in nitrogen.

Synthesis

Synthesis of 4,4'-((DOPO)methylene)diphenol (1a). Figure 1a shows the reaction process. DOPO (10.809g, 0.05mol), p-hydroxybenzaldehyde (6.106g, 0.05mol), phenol (22.528g, 0.25mol), and p-TSA (0.432g, 4.0wt% of DOPO) were added to 250ml three-way flask. The mixture was stirred at 130℃ for 24h in a nitrogen atmosphere. After stopping the reaction, it was cooled to room temperature. The precipitate was then filtered and washed with ethanol to remove excess phenol.

After vacuum drying, a white solid was obtained.[1]H NMR (400 MHz, DMSO) δ 9.39 (d, J = 11.4 Hz, 2H), 8.13 (dd, J = 12.3, 5.6 Hz, 2H), 7.68 (t, J = 7.4 Hz, 1H), 7.49 – 7.36 (m, 3H), 7.32 (t, J = 7.6 Hz, 1H), 7.25 (d, J = 6.9 Hz, 2H), 7.15 (d, J = 6.8 Hz, 2H), 7.06 (d, J = 8.1 Hz, 1H), 6.66 (dd, J = 8.7, 2.5 Hz, 4H), 4.45 (d, J = 15.6 Hz, 1H).

Synthesis of 4-((4-hydroxyphenyl)(DOPO)methyl)-2-methylphenol (1b). This compound was prepared according to the same procedure for synthesizing 1a using o-cresol (27.035g, 0.25mol) as starting material. 1H NMR (400 MHz, DMSO-D6) δ 9.39 (d, J = 17.4 Hz, 1H), 9.28 (d, J = 19.8 Hz, 1H), 8.16 – 8.08 (m, 2H), 7.68 (t, J = 7.6 Hz, 1H), 7.49 – 7.38 (m, 3H), 7.35 – 7.30 (m, 1H), 7.24 (d, J = 7.1 Hz, 1H), 7.15 – 7.10 (m, 1H), 7.08 – 7.04 (m, 1H), 7.00 (s, 1H), 6.94 (d, J = 8.2 Hz, 1H), 6.65 (ddd, J = 9.8, 8.2, 5.7 Hz, 3H), 4.44 – 4.34 (m, 1H), 2.02 (s, 3H).

Synthesis of O,O'-(((DOPO)methylene)bis(4,1-phenylene))bis(dimethylcarbamothioate)（2a）. Monomer 1a (10.3600g, 0.025mol) and DABCO (11.2170g, 0.1mol) were dissolved in DMF (100ml) in a 250ml flask. Under N_2 atmosphere, the mixture was stirred until completely dissolved. Then DMTCC (12.3604g，0.1mol) was added. Stir at room temperature overnight. Pour ice water to quench the reaction. The solid was collected via filtration, washed with water several times, and then dried under vacuum to obtain the product as a light yellow solid.[1]H NMR (400 MHz, DMSO) δ 8.21 – 8.12 (m, 2H), 7.72 (dt, J = 8.3, 4.4 Hz, 1H), 7.56 – 7.50 (m, 2H), 7.48 – 7.32 (m, 6H), 7.00 (d, J = 8.4 Hz, 5H), 4.86 (d, J = 15.1 Hz, 1H), 3.33 (s, 12H).

Synthesis of O-(4-((4-((dimethylcarbamothioyl)oxy)phenyl)(DOPO)methyl)-2-methylphenyl) dimethylcarbamothioate（2b）. Compound 2b was prepared using the same procedure for synthesizing 2a using 1b as starting material, then purified with silica gel column chromatography to afford compound 2b. [1]H NMR (400 MHz, DMSO) δ 8.18 (d, J = 7.7 Hz, 2H), 7.73 (t, J = 8.3 Hz, 1H), 7.53 (d, J = 8.5 Hz, 1H), 7.49 – 7.31 (m, 6H), 7.27 (s, 1H), 7.09 – 6.96 (m, 3H), 6.92 (t, J = 8.1 Hz, 1H), 4.79 (dd, J = 15.1, 11.1 Hz, 1H), 3.35 (d, J = 5.0 Hz, 6H), 3.30 (d, J = 7.6 Hz, 6H), 2.04 (d, J = 3.3 Hz, 3H).

Synthesis of S,S'-(((DOPO)methylene)bis(4,1-phenylene))bis(dimethylcarbamothioate)(3a). Monomer 2a (7.0053g, 11.9mmol) and diphenyl ether (20g) were added to a 50ml three-way flask and reacted for 2h at 260℃ in N_2 atmosphere. After completion of the reaction, the mixture was cooled to room temperature and washed several times with methanol. Then the solid was recrystallized with dichloromethane and methanol to obtain 4.9573g of white powder (Yield: 70.76%).[1]H NMR (400 MHz, DMSO) δ 8.18 (d, J = 8.1 Hz, 2H), 7.74 (t, J = 7.8 Hz, 1H), 7.58 (d, J = 8.3 Hz, 2H), 7.54 – 7.30 (m, 10H), 7.08 (d, J = 6.0 Hz, 1H), 4.99 (d, J = 14.9 Hz, 1H), 2.97 (d, J = 44.7 Hz, 12H).

Synthesis of S-(4-((4-((dimethylcarbamoyl)thio)-3-methylphenyl)(DOPO)methyl)phenyl) dimethylcarbamothioate(3b). 3b is prepared like 3a and then purified with silica gel column chromatography to afford compound 3b. [1]H NMR (400 MHz, DMSO) δ 8.17 (dd, J = 8.2, 3.9 Hz, 2H), 7.73 (t, J = 7.7 Hz, 1H), 7.61 – 7.20 (m, 11H), 7.08 (d, J = 8.0 Hz, 1H), 4.91 (dd, J = 14.9, 12.5 Hz, 1H), 3.03 (d, J = 9.5 Hz, 6H), 2.91 (s, 6H), 2.23 (s, 3H).

Synthesis of 4,4'-((DOPO)methylene)dibenzenethiol (BMDO). 7.08g (0.108mol) 85% KOH was dissolved in 0.42ml water and 20.4ml methanol. Then monomer 3a (7.0642g, 12mmol) was added. The mixture was refluxed for 2h. After the reaction finished, the solution was diluted to 108mL with water, then 13.2mL hydrochloric acid was added. The suspension was filtered out and vacuum dried to produce the white powder. [1]H NMR (400 MHz, DMSO) δ 7.93 – 7.75 (m, 1H), 7.45 (t, J = 7.6 Hz, 1H), 7.30 (t, J = 7.7 Hz, 3H), 7.19 – 6.96 (m, 10H), 6.89 (d, J = 7.1 Hz, 1H), 5.30 (s, 2H), 3.96 (d, J = 17.1 Hz, 1H).

Synthesis of 4-((4-mercaptophenyl)(DOPO)methyl)-2-methylbenzenethiol (OBMDO). The preparation process of OBMDO is similar to that of BMDO, using 3b as the starting material. [1]H NMR (400 MHz, DMSO) δ 7.83 (dq, J = 17.4,

10.2, 8.4 Hz, 1H), 7.44 (d, J = 7.5 Hz, 1H), 7.38 – 7.25 (m, 3H), 7.23 – 6.98 (m, 8H), 6.92 (dd, J = 16.1, 7.0 Hz, 2H), 5.27 (d, J = 12.4 Hz, 1H), 5.02 (d, J = 15.9 Hz, 1H), 3.94 (qd, J = 20.3, 19.2, 9.1 Hz, 1H), 2.10 (d, J = 15.2 Hz, 3H).

Synthesis of 2,2',2''-((phenylsilanetriyl)tris(oxy))tris(ethane-1-thiol)(PSTS). The reaction process is shown in Figure 1b. The diethyl ether (400mL), triethylamine (18.2 mL, 0.13mol), and 2-mercaptoethanol (9.20mL, 0.13mol) were put into a 3-necked 1L round-bottled flask. Stir and cool the solution in an ice bath under N_2 atmosphere. Add phenyl trichlorosilane (7.00mL, 0.044mol) slowly to the agitated solution. The suspension was gradually heated to room temperature and stirred overnight in N_2 atmosphere. The suspension was filtered with ether as a washing solution. Rotary evaporation was used to remove all volatiles from the filtrate to obtain the oil. Then the oil was purified by reduced pressure distillation to obtain a clear, colorless liquid. ^{1}H NMR (400 MHz, $CDCl_3$) δ 7.70 – 7.43 (m, 3H), 7.37 – 7.28 (m, 2H), 3.83 (dt, J = 12.0, 6.4 Hz, 6H), 2.58 (ddt, J = 17.5, 8.5, 6.5 Hz, 6H), 1.53 – 1.33 (m, 3H).

Synthesis of vinyl oligosiloxane resins (PVO). MVDMS and DPSD were the precursors for synthesizing linear vinyl oligo-siloxane resins. Barium hydroxide monohydrate was added as an alkaline catalyst (0.1mol% of all silane precursors). Organosilicon resins were synthesized by sol-gel method using MVDMS and DPSD (molar ratio of 1:1). The reactants were mixed and stirred at 80℃ for 8 h. The oligomer was filtered through a 0.45mm Teflon filter to remove the catalyst. Then, volatile components were removed by vacuum heating. The final obtained PVO was 0.003 mol/g of vinyl content. The schematic illustration for the synthesis of PVO oligomer was given in Scheme 1c.

Preparation of the Siloxane−Sulfide Polymer Films. Scheme 1d shows the cross-linking network formed by the thiol-ene reaction of silicone resin. The curing preparation process is as follows: A certain amount of dopants (BMDO and OBMDO) were dissolved in PSTS and then mixed with PVO in an equal molar ratio of vinyl and sulfhydryl group. Then add 184 photoinitiator (0.2wt% of the total amount), stir well, defoaming under vacuum, and pour into the Teflon mold with glass sheets on the top and bottom. After curing in UV curing box for 10min, the colorless and transparent organosilicon film was obtained. The molar ratio of the reacting functional groups in PSTS and PVO is 1:1, meaning the mass ratio is 1:3. Depending on the content and type of dopant, these polymers are called SV, SBV, and SOV. The specific curing compound names, chemical composition details and measured Shore hardness are given in Table 1.

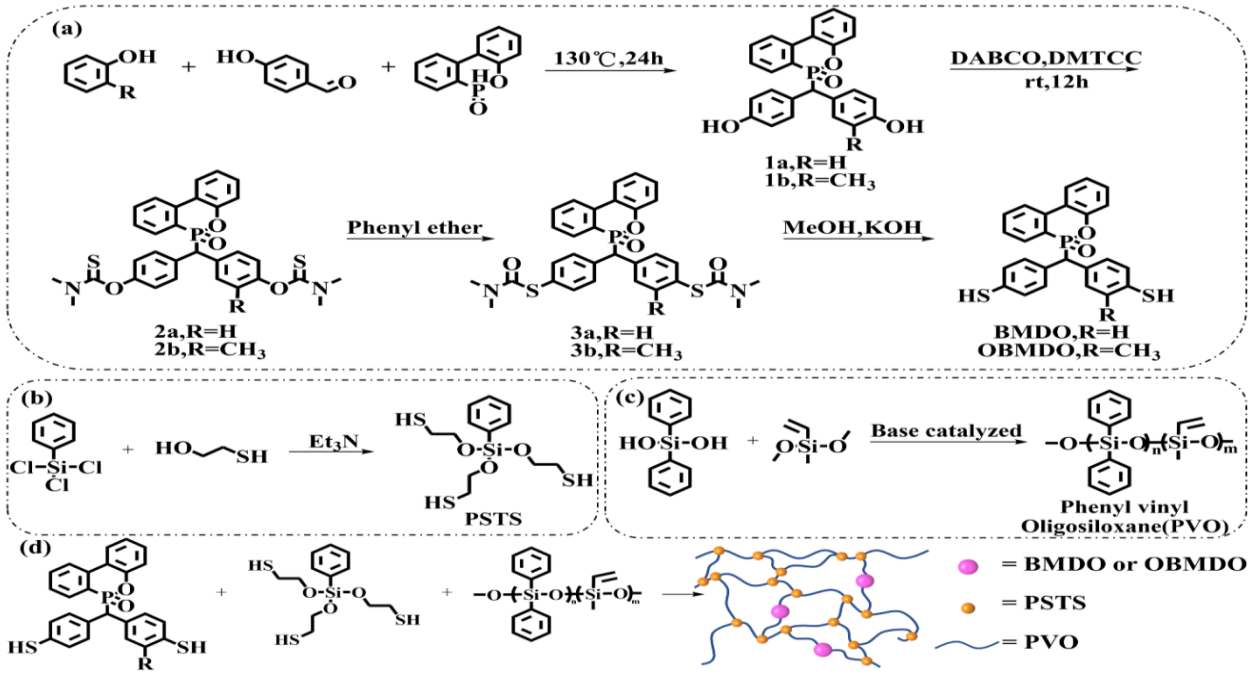

Scheme 1 Synthetic route of BMDO and OBMDO (a), PSTS (b), PVO (c), and crosslinking reaction (d).

Table 1 Chemical composition, mechanical and optical properties of cured product.

Sample	Weight ratio			Hardness (Shore D)	Refractive index	T% at 470nm	
	PVO : PSTS	BMDO	OBMDO			Initial	48h [a]
SV	3 : 1	——	——	56	1.5773	96.58	95.63
SBV-1	3 : 1	0.01	——	62	1.5782	93.31	91.10
SBV-3	3 : 1	0.03	——	53	1.5795	89.60	84.75
SBV-5	3 : 1	0.05	——	49	1.5807	86.14	78.78
SOV-1	3 : 1	——	0.01	59	1.5777	92.88	90.43
SOV-3	3 : 1	——	0.03	55	1.5789	92.82	90.85
SOV-5	3 : 1	——	0.05	53	1.5803	91.43	88.49

[a] Samples had been baked at 150 °C for 48h

Result and discussion

The synthesis of a new crosslinking agent is an important way to prepare room-temperature vulcanized silicone rubber. In this work, the bisthio compounds (BMDO and OBMDO) and the trithione compound (PTST) were prepared through the Newman-Kwart rearrangement and hydrolysis reactions. The methyl vinyl phenyl silicone resin was obtained simply through non-hydrolytic sol-gel reaction. The silicone rubber with a high refractive index were successfully synthesized through the free radical addition reaction between the -SH bond of the crosslinker and silicone oligomers containing vinyl. The thiol-ene reaction is a stepwise addition polymerization reaction. Under the action of the photoinitiator, the sulfur radical on the sulfhydryl group attacks the carbon atom on the double bond, making the other carbon atom a new free radical.

Synthesis and characterization

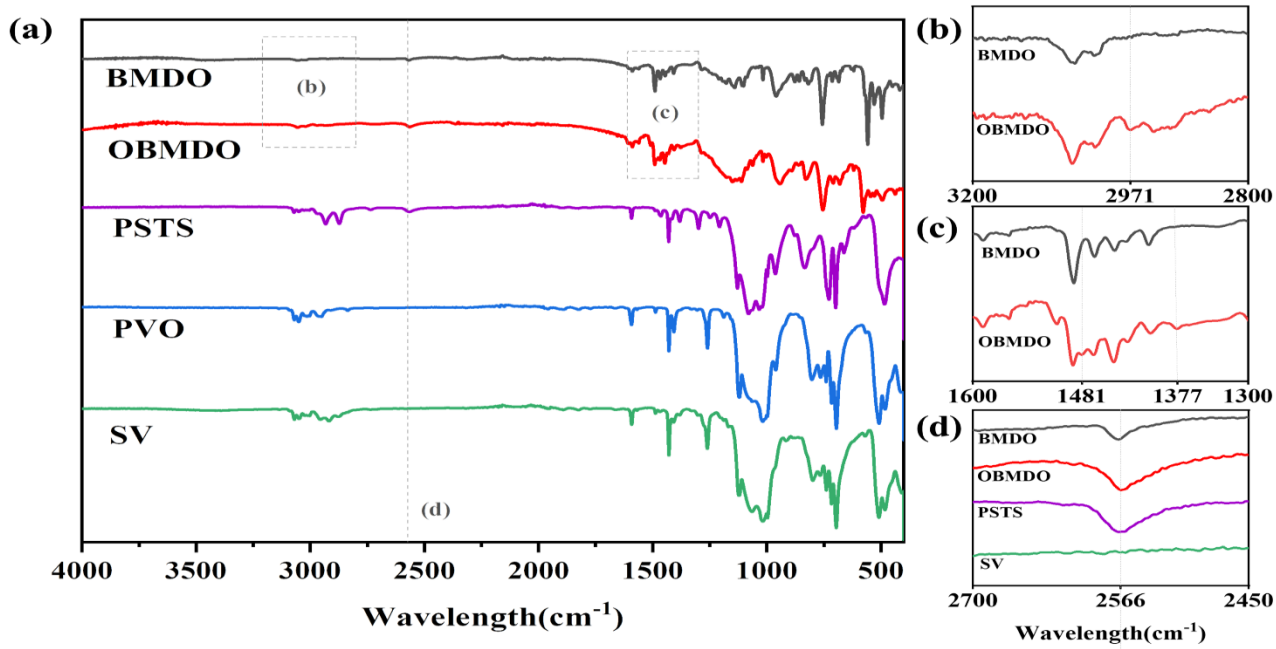

Figure 1. (a) FT-IR spectra of BMDO, OBMDO, PSTS, PVO and SV; (b) FT-IR spectra of BMDO and OBMDO at 3200cm^{-1} to 2800cm^{-1}; (c) FT-IR spectra of BMDO and OBMDO at 1600cm^{-1} to 1300cm^{-1}; (d) FT-IR spectra of BMDO, OBMDO, PSTS and SV at 2700cm^{-1} to 2450cm^{-1}.

The BMDO, OBMDO, PSTS, and PVO chemical structures were characterized by IR (Figure 1). The signals of the P=O and P-Ph vibration of BMDO and OBMDO are at 1284cm^{-1} and 1485cm^{-1}, respectively, while the stretching vibration of the P-O-Ph are around 1141cm^{-1} and 1013cm^{-1}. The methyl peak in OBMDO is located at 2971cm^{-1}, 1377cm^{-1}, and 1481cm^{-1} (Figure 1b and 1c). The peak at 1000cm^{-1} to 1080cm^{-1} belongs to the stretching vibration of the Si-O-Si bond of organosilicon polymer. After the sol-gel reaction, silanol (peak at 3650cm^{-1}, Si-OH) in DPSD does not remain, so the condensation reaction is fully completed. 3070cm^{-1}, 1593cm^{-1}, 1429cm^{-1} and 1120cm^{-1} are the peaks of Si-Ph. The peak at 2933 cm^{-1} is attributed to the stretching vibration absorption peak of -CH_2-. The peak at 2566 cm^{-1} in the FT-IR spectrum of PSTS, BMDO, and OBMDO represents the sulfhydryl group. The disappearance of the sulfhydryl peak after curing (Figure 1d) indicates that the curing reaction has been completed.

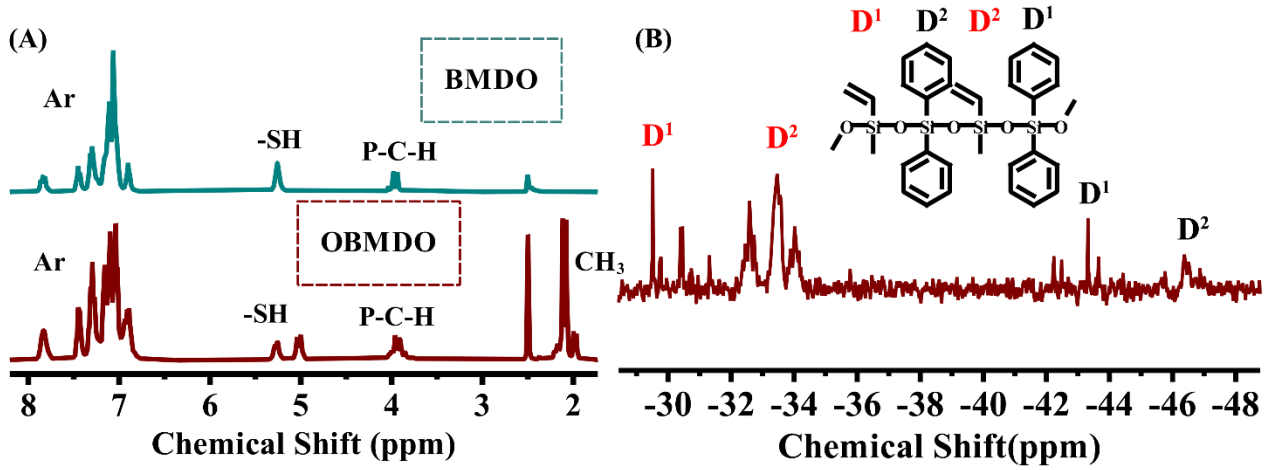

Figure 2. (a) ^{1}H-NMR spectra of BMDO and OBMDO; (b) ^{29}Si-NMR spectra of PVO1.

Figure 2a shows the ^{1}H-NMR spectra of BMDO and OBMDO. The characteristic sulfhydryl group peak of the BMDO located at 5.2 ppm. In the case of OBMDO, the two peaks assignable to the sulfhydryl group at 5.0 ppm and 5.2 ppm were observed because of the nearby methyl. The P-C-H peak was found at 3.9 ppm as well.

The D^n could be used to analyze the Si atom of silane with two siloxy groups, in which the n represents the number of siloxane bonds linked to the Si atom. The silicone resin contains only the D^n material in the MVDMS (red) and DPSD (black) precursors, resulting in a linear connection of siloxane bonds. D^2 represents condensation into two siloxane bonds without any remaining methoxyl or silanol groups. And large quantities of D^2 substances (-32 to -35 ppm and -42 to -47 ppm) were detected. According to eq.1, the calculated condensation degree (DOC) of silicone resin is 92.0%

$$Degree\ of\ condensation = \frac{D^1+2D^2}{2(D^1+D^2)} \quad \text{eq.1}$$

The results of this study indicate that successful synthesis of BMDO, OBMDO and PSTS. The resulting PSTS has low viscosity. And BMDO and OBMDO is soluble in PSTS, which is easily processed.

Study on photoelectric properties of curing compounds

The transmittance of the films at different wavelengths is shown in Figure 3. The cured material with different dopant contents can be seen to have a high transmittance (greater than 90%) at the 500-800nm level. As the dopants' content is increased, the transmittance rate of the cured material decreases at 350-500nm. The transmittal rate of SV at 470nm is 96%, while the SBV-5 is 86%. In general, the transparency of polymer materials is affected by the compatibility between materials, the crystallinity of materials, and the uniformity of crosslinking networks. Thus, the poorer transparency of the SBV-5 can be attributed to the formation of aggregation because of the poor compatibility between the large conjugated groups of BMDO and the siloxane monomer in SBV-5. Meanwhile, comparing the cured substance doped with BMDO

and OBMDO, it can be found that the optical transmittance of the cured substance doped with OBMDO is higher at the same content. This is due to the asymmetrical structure of the doped monomer, which makes the conjugated groups less likely to aggregate and leads to the formation of scattering centers. As a result, the optical transmittance of the OBMDO-doped cured substance is higher. Besides, the transmittance spectra of the samples after thermal aging at 150℃ for 48h were monitored to evaluate the thermal resistance of the cured film. It can be seen from figure 3 that the UV absorption in the sample increases incrementally with aging time.

The curing material described in this paper is completed by a thiol-ene reaction. The choice and amount of photoinitiator is crucial to obtain a colorless and transparent material. The themal behavior of the photoinitiator could be used to evaluate the reactivity of the photoinitiator for this reaction. Our result indicate that 1wt% loading of the photoinitiator is appropriate for experimental screening[37]. Although increasing the initiator content may improve the rate of reaction, the colour and light transmittance of the cured material will be affected by the residual catalyst. Moreover, the appearance of the cured substance gradually turns yellow with increasing the loading of the photoinitiator.

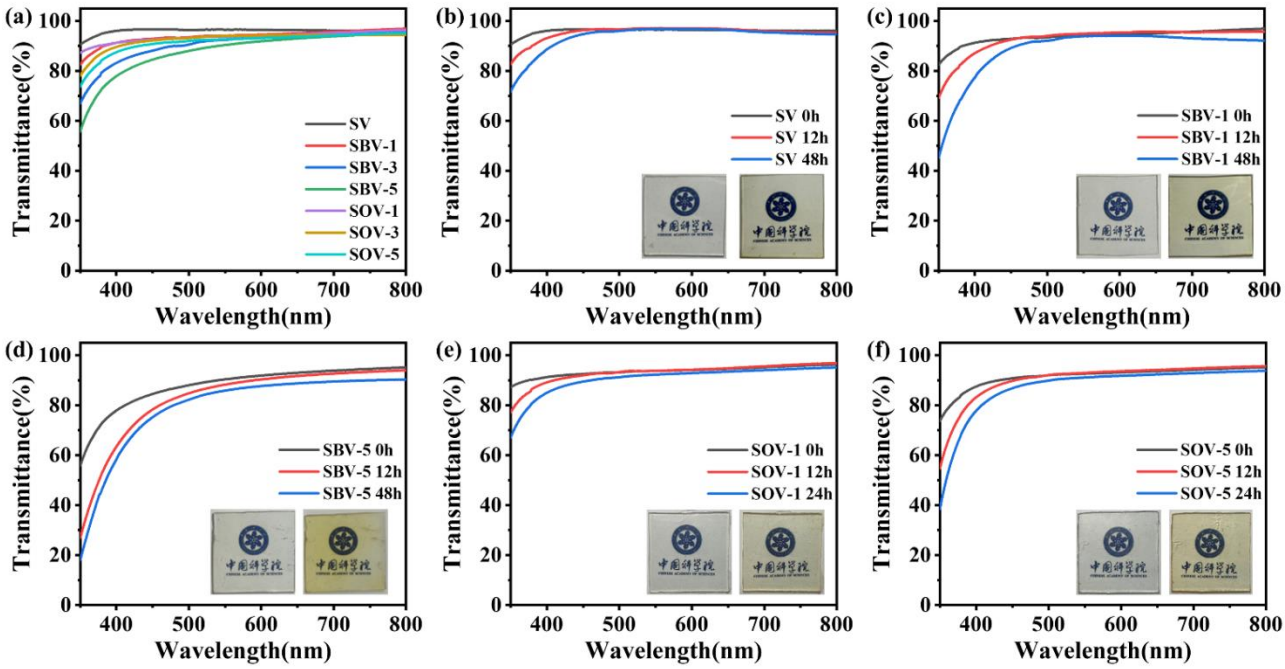

Figure 3. (a) Transmittance spectra of all cured film; (b-f) Transmittance spectra and optical images of different samples before (black line) and after thermal aging at 150℃ for 12h (red line) and 48h (blue line).

The refractive index of the cured substance

The refractive index may be improved by increasing the molecular or group polarizability or by reducing the molecular molar volume. Large conjugated groups as well as S and P heteroatoms were introduced into the resin in order to increase the electron polarization and improve the refractive index of the resin. The refractive indices of the cured films were assessed by an Abbe refractometer (Table 1). As the dopant content increases, the index of refraction of the hybrid resin increases from 1.5773 to 1.5807. No huge the refractive index difference was observed between BMDO-doped and OBMDO-doped cured products. According to the Lorentz-Lorenz formula, the refractive index of a material is related to electron polarization and density.

Thermo-mechanical properties of cured materials

Plots of the energy storage modulus and loss factor (tanδ) of four silicone cured compounds as a function of temperature are shown in Figure 4. The glass transition temperature of the cured substance is taken as the peak temperature of *tanδ*, and

the specific data are shown in Table 2.

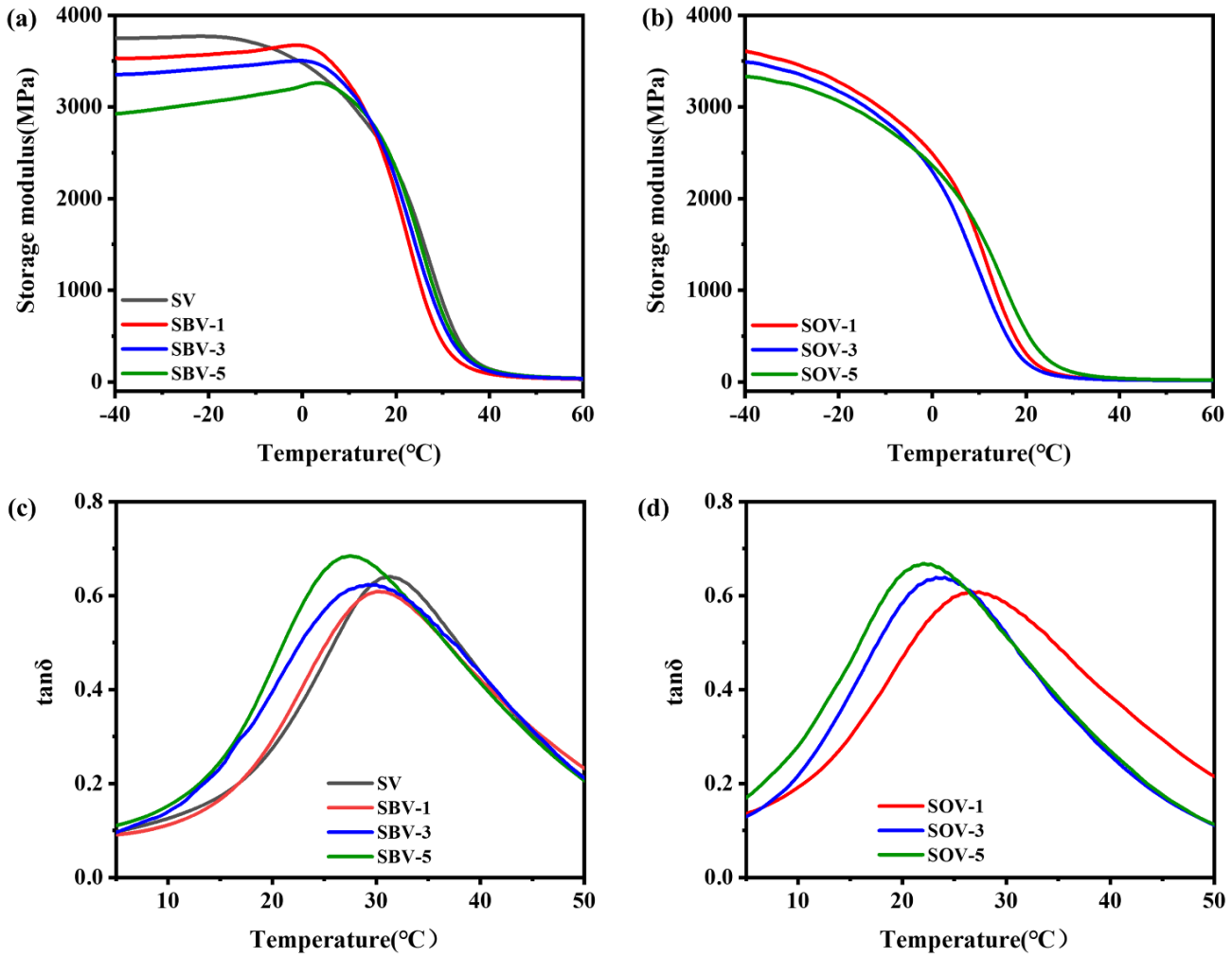

Figure 4. DMA curves of the cured films in N_2 atmosphere; (a, b) Storage modulus curves of SV, SBV and SOV; (c, d) Loss tangent curves of SV, SBV and SOV.

In order to explain the influence of the molecular structure on the stiffness of the corresponding lattice, this plot shows the relationship between the temperature as a function of the energy storage modulus (E') and the loss factor ($tan\delta$) for different samples. As can be seen, with increasing dopant content, the energy storage modulus in the glassy region initially decreases and then increases, which can be related to the crosslinking density of the silicone lattice. Based on the elastic modulus of rubber calculated, the cross-link density of each system using eq.2

$$E_r=3RT_r\gamma_e \quad \text{eq.2}$$

Where E_r is the energy storage modulus in the rubber region, which can be regarded as T_g+30, R is the universal gas constant, T_r is the temperature corresponding to E_r, and γ_e is the crosslinking density.

SBV-1 is calculated to have the highest crosslink density (Table 3). Due to a large number of bulky phenyl groups adjacent to the vinyl group in silicone, the movement of the backbone is limited to a certain extent. The restricted movement of the skeleton is not conducive to effective collision with the cross-linking agent, which will lead to a cross-linked network with certain defects. As the dopant content is increased, a portion of the three-functional crosslinking agent is replaced by the two-functional compounds. As a result, the crosslinking points are more dispersed, and efficient collisions are more likely to occur, leading to an increase in crosslinking density. Thus, SBV-1 has a higher crosslink density than that of the SV. Meanwhile, the SOV-1 has a lower crosslinking density than that of the SBV-1. This is probable due to the increased

resistance of the spatial site caused by the nearby methyl group in OBMDO. This interferes with the efficient collision between sulfhydryl and vinyl groups, resulting in a lower cross-linking density with a greater number of defects. From the Fig. 4a, it can be observed that the storage modulus of our silicone resins changes accordingly with contents of dopants in the glassy state. The SV displayed the highest storage modulus , though its crosslink density is minor than that of the SBV-1. It may be attributed to the lower crosslinking points in the crosslinking network which is favour for the stacking of molecular chain segments.

At the same time, increasing the dopant content lowers the glass transition temperature (T_g) of our cured product. The presence of T_g is usually attributed to segmental movement of the polymer network. The value of T_g is determined by the degree of freedom of segmental movement, crosslink density, entanglement constraints, and the stacking density of the segments[38]. The *Tan* δ_{max} first decreases and then increases with increasing of the BMDO content (Figure 4c). Lower peaks correspond to higher crosslinking density, resulting in more restricted segment motion and mobility. The SBV-1 has a higher crosslinking density than that of the SV and thus more crosslinking points restrict the motion of the molecular chain segments in the crosslinking network. However, the enormous molecular volume of BMDO can also expand the intermolecular space and improve the motility of the segments, leading to a lower T_g. Due to the lower crosslink density of SOV-1 compared to SBV-1, as well as the larger molecular size of OBMDO compared to BMDO, the T_g of the SOV-1 is lower than that of the SBV-1. In case of the OBMDO doped products, T_g of SOV-1 than that of SBV-1 because the molecular size of OBMDO is higher than that of BMDO. The full width at half maximum (FWHM) of the loss factor peak can reflect the uniformity of the cross-linked network. The larger the FWHM, the wider the distribution of molecular chain length between cross-linking points, and the more uneven the cross-linking network. With the introduction of dopants, the number of large conjugated groups in the molecule increases, affecting the formation of the cross-linked network. The dopants and PSTS have inconsistent functional groups, leading to random cross-linking. Therefore, the network formed after introducing dopants will be prone to defects, and the distribution of molecular chains between the crosslinking sites is not uniform. Therefore, the FWHM of SV is wider than those of others cured product.

The resulting crosslinking density (γ_e), glass transition temperature (T_g), and energy storage modulus (E') are summarized in Table 2. The results show that the crosslinking density of SBV-1 is the highest. This increased density of crosslinks is due to more efficient crosslink points in the network and a shorter average length of chain between the crosslinks. And the increase in crosslink density also makes viscoplastic deformation of the network more difficult, thus reducing elastic energy dissipation during cooperative motion of the whole SBV-1 network chain under stress.

Table 2 Summarized some characteristic data from DMA spectra.

Sample	α-relaxation (T_g)/℃	Rubber modulus at T_g+30℃/MPa	Cross-link desity (γ_e)/mol·m^{-3}
SV	31.44	24.01	2878
SBV-1	30.21	24.64	2965
SBV-3	27.49	21.2	2572
SBV-5	23.92	19.82	2431
SOV-1	26.50	22.26	2709
SOV-3	24.09	18.93	2320
SOV-5	21.91	17.80	2196

Thermal stability of silicone-cured products

The TGA and DTG were used to characterize the thermal stability of different silicone curing materials (Figure 5). A summary of the corresponding decomposition data including $T_{5\%}$, T_{max} and char yield at 800℃ are shown in Table 3. In general, the heat resistance of polymer materials depends on the crosslinking density and molecular chain rigidity. The thermogravimetric analysis studied the relationship between the thermal degradation performance of silicone resin and the

content of dopants. All 5% thermal weight loss of our silicone curing materials exceed 300℃, indicating that the silicon material synthesized in this paper has good thermal resistance.

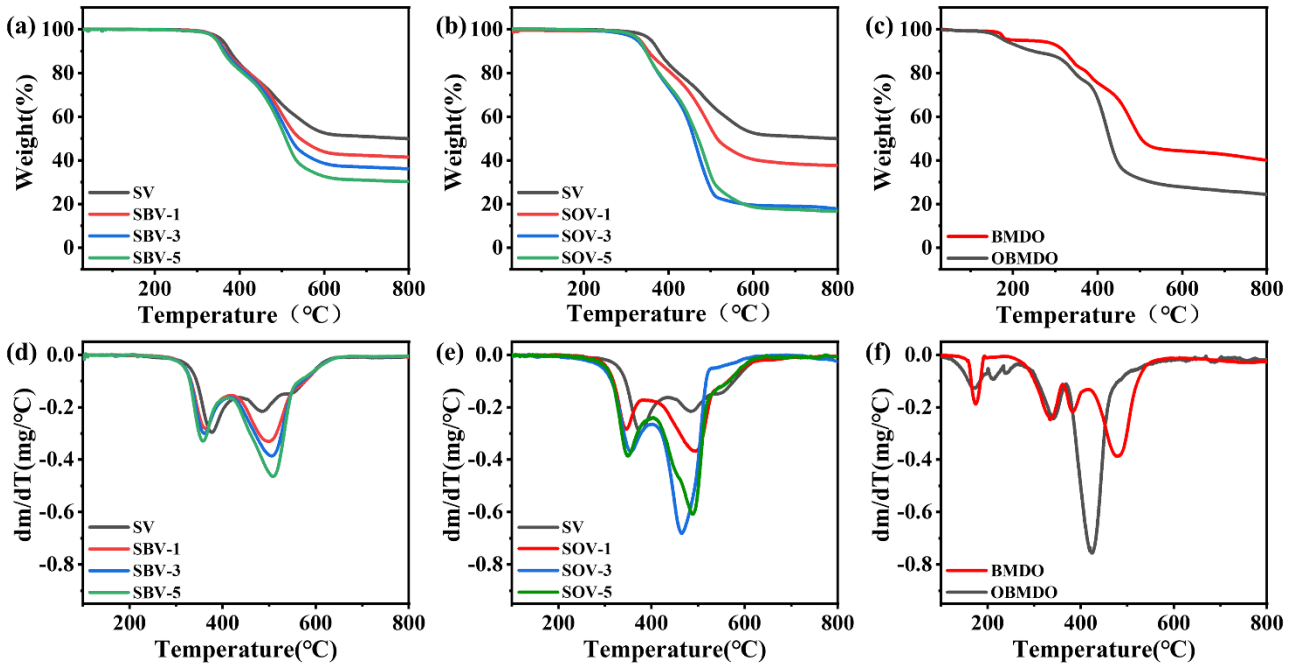

Figure 5. TGA curves of cured resin composites SBV (a), SOV (b) and monomers (c); DTG curves of cured resin composites SBV (a), SOV (b) and monomers (c).

Comparing the cured compounds with different contents of dopant, it can be found that the increase of the dopants' loading could effectivley decrease the maximum decomposition rate of cured products (Table 3). The 5% weight loss temperature of SBV-1 is at 350℃, while that of the SBV-5 is around 346℃. This relatively low thermal stability can be attributed to the decomposition of BMDO at a lower temperature. The gradual decrease of $T_{5\%}$ and T_{max} was mainly attributed to the decomposition of phosphorus groups (mainly caused by the weak P-O-C bond). Despite more rigid structures in the SBV-5 system, more defects exist in the SBV-5. The introduction of bulky groups into polymer backbones destroys their overall structure, leading to a decrease in heat resistance. Comparing to SBV-1, the thermal stability of SOV-1 is lower becuase of its lower crosslink density. Meanwhile, the asymmetric structure of OBMDO also affects the thermal stability of the cured product. The decomposition temperature of OBMDO is lower than that of BMDO. As the DTG (Figure 5d) shows, two degradation peaks indicate different decomposition mechanisms for silicone rubber. With the increase of the content of BMDO, the peak intensity at 500℃ increased gradually, and residual char decreased. The decrease of residual char is due to the decomposition of the P-containing groups that create highly reactive P radical species. The first degradation step may correspond to the decomposition of structures such as organosilicon network, while the second degradation step may be related to dopants. Polysiloxanes undergo progressive degradation of the main chain and oxidation of the methyl group above 300℃. The thermal degradation of polysiloxanes occurs through the depolymerization of Si-O rearrangement, creating cyclic oligomers. Since the silicone oligomers have abundant vinyl side groups, it can disrupt the convoluted helical structure of polysiloxanes. The tri-functional crosslinker can make the crosslinking network more tightly. The cross-linker agent reacts with the vinyl to form T-shaped structural units, creating a dense network. The dense network can restrict the movement of Si-O-Si chain segments. Thus, branched chains and T-shaped structures in silicones can prevent the rearrangement of Si-O bonds in polysiloxanes and the formation of cyclic oligomers. In addition, at high temperatures, Si-CH_3 bond breakage will form some free radicals, and these large radicals may also be cross-linked by

mutual coupling. The cross-linked network of steric hindrance and large free radicals reduces the flexibility of organosilicon chains, preventing cyclic oligomers from further splitting and retarding further degradation of Si-O-Si chains. The dopant degrades sharply at 400°C, which leads to a break in the cross-linked network of the cured product. This creates smaller molecular weight chain segments, intensifying the cured substance's decomposition and reducing the residual char.

Table 3 TGA Result of cured compounds

Sample	$T_{5\%}$ (°C)[a]	T_{max} (°C)[b]	R_w (%)[c]
SV	358	375	50
SBV-1	350	497	42
SBV-3	348	506	36
SBV-5	346	511	30
SOV-1	333	495	38
SOV-3	330	488	18
SOV-5	325	465	17
BMDO	212	480	40
OBMDO	179	424	24

[a] The temperature is at 5% loss.

[b] The temperature of maximum weight loss rate.

[c] Residual char at 800°C.

Conclusion

BMDO and OBMDO were successfully synthesized. HRIP were prepared using PTST and BMDO (or OBMDO) as cross-linking agents to react with PVO. In addition, HRIP has a relatively high Shore D hardness. The results showed that the refractive indices of SBV and SOV were higher than SV besides their optical transmittance were also higher than 90%. The asymmetric nature of OBMDO makes it less likely to agglomerate in the cured material, resulting in a higher light transmission rate for SOV than SBV. DMA data shows that adding too much BMDO and OBMDO will decrease crosslink density and T_g. It can be seen from the TGA that the higher the dopant content, the lower the $T_{5\%}$, T_{max}, and residual char, and the lower the thermal stability. However the thermal decomposition temperatures are all above 300°C, meeting the requirements of most environments.

Acknowledgments

This work was supported by the Fujian Science and Technology Innovation Laboratory for Optoelectronic Information of China (2021ZZ107) and the Science and Technology Service Network Plan of Chinese Academy of Sciences (2023T3093).

Data sharing agreement

The datasets used and analyzed during the current study are available from the corresponding author on reasonable request.

Declaration of Conflicting Interests

The authors declared no potential conflicts of interest with respect to the research, author-ship, and publication of this article.

References

[1]. 1 Xibing Zhan, X. Cai and J. Zhang, *RSC Adv.*, 2018, **8**, 12517-12525.

[2]. 2 E. Yilgör and I. Yilgör, *Prog. Polym. Sci.*, 2014, **39**, 1165-1195.

[3]. 3 S.C. Shit and P. Shah, *National Academy Science Letters*, 2013, **36**, 355-365.

[4]. 4 M. Ma, F.W. Mont, D.J. Poxson, J. Cho, E.F. Schubert, R.E. Welser and A.K. Sood, *J. Appl. Phys.*, 2010, **108**, 43102.

[5]. 5 E. Wrzesniewski, S. Eom, W. Cao, W.T. Hammond, S. Lee, E.P. Douglas and J. Xue, *Small*, 2012, **8**, 2647-2651.

[6]. 6 J. Bae, Y. Kim, H. Kim, Y. Lim and B. Bae, *RSC Adv.*, 2013, **3**, 8871.

[7]. 7 D.W. Mosley, G. Khanarian, D.M. Conner, D.L. Thorsen, T. Zhang and M. Wills, *J. Appl. Polym. Sci.*, 2014, **131**, n/a-n/a.

[8]. 8 W. Zhang and A.H.E. Müller, *Prog. Polym. Sci.*, 2013, **38**, 1121-1162.

[9]. 9 S. Xiao, M. Nguyen, X. Gong, Y. Cao, H. Wu, D. Moses and A.J. Heeger, *Adv. Funct. Mater.*, 2003, **13;10**, 25-29.

[10]. 10 C. Zhang, F. Babonneau, C. Bonhomme, R.M. Laine, C.L. Soles, H.A. Hristov and A.F. Yee, *J. Am. Chem. Soc.*, 1998, **120**, 8380-8391.

[11]. 11 E.K. Macdonald and M.P. Shaver, *Polym. Int.*, 2015, **64**, 6-14.

[12]. 12 Y. Tang, Z. Li, Z. Li, J. Li, S. Yu and L. Rao, *IEEE T. Electron Dev.*, 2018, **65**, 158-164.

[13]. 13 A.W. Ritchie, H.J. Cox, H.I. Gonabadi, S.J. Bull and J.P.S. Badyal, *ACS Appl. Mater. Inter.*, 2021, **13**, 33477-33484.

[14]. 14 S. Mahendia, A. Kumar Tomar, P.K. Goyal and S. Kumar, *J. Appl. Phys.*, 2013, **113**, 73103.

[15]. 15 P.M. Reddy, C. Chang, C. Lai, M. Su and M. Tsai, *Compos. Sci. Technol.*, 2018, **165**, 95-105.

[16]. 16 H. Kochkar and F. Figueras, *J. Catal.*, 1997, **171**, 420-430.

[17]. 17 R. Murugavel, A. Voigt, M.G. Walawalkar and H.W. Roesky, *Chem. Rev.*, 1996, **96**, 2205-2236.

[18]. 18 S. Yang, J. Kim, J. Jin, S. Kwak and B. Bae, *J. Appl. Polym. Sci.*, 2011, **122**, 2478-2485.

[19]. 19 P.T. Chung, C.T. Yang, S.H. Wang, C.W. Chen, A.S.T. Chiang and C. Liu, *Mater. Chem. Phys.*, 2012, **136**, 868-876.

[20]. 20 P. Tao, Y. Li, R.W. Siegel and L.S. Schadler, *J. Appl. Polym. Sci.*, 2013, **130**, 3785-3793.

[21]. 21 C. Tsai and G. Liou, *Chem. Commun.*, 2015, **51**, 13523-13526.

[22]. 22 J. Kim, S. Yang and B. Bae, *Chem. Mater.*, 2010, **22**, 3549-3555.

[23]. 23 *Journal of macromolecular science. Part A, Pure and applied chemistry*, 2015, **52**, ebi-ebi.

[24]. 24 E. Goosey, *Circuit World*, 2006, **32**, 32-35.

[25]. 25 R.A. Minns and R.A. Gaudiana, *Journal of macromolecular science. Part A, Pure and applied chemistry*, 1992, **29**, 19-30.

[26]. 26 R.A. GAUDIANA and R.A. MINNS, *JOURNAL OF MACROMOLECULAR SCIENCE-CHEMISTRY*, 1991, **A28**, 831-842.

[27]. 27 S. Liu, M.D. Islam, Z. Ku, D.A. Boyd, Y. Zhong, A.M. Urbas, E. Smith, J. Derov, V.Q. Nguyen, W. Kim, J.S. Sanghera, Y. Ko, J. Genzer, X. Ye, Z. Guo, E. Seo and J.E. Ryu, *Composites Part B: Engineering*, 2021, **223**, 109128.

[28]. 28 T.S. Kleine, N.A. Nguyen, L.E. Anderson, S. Namnabat, E.A. LaVilla, S.A. Showghi, P.T. Dirlam, C.B. Arrington, M.S. Manchester, J. Schwiegerling, R.S. Glass, K. Char, R.A. Norwood, M.E. Mackay and J. Pyun, *ACS Macro Lett.*, 2016, **5**, 1152-1156.

[29]. 29 L.E. Anderson, T.S. Kleine, Y. Zhang, D.D. Phan, S. Namnabat, E.A. LaVilla, K.M. Konopka, L. Ruiz Diaz, M.S. Manchester, J. Schwiegerling, R.S. Glass, M.E. Mackay, K. Char, R.A. Norwood and J. Pyun, *ACS Macro Lett.*, 2017, **6**, 500-504.

[30]. 30 J.J. Griebel, S. Namnabat, E.T. Kim, R. Himmelhuber, D.H. Moronta, W.J. Chung, A.G. Simmonds, K. Kim, J.

van der Laan, N.A. Nguyen, E.L. Dereniak, M.E. Mackay, K. Char, R.S. Glass, R.A. Norwood and J. Pyun, *Adv. Mater.*, 2014, **26**, 3014-3018.

[31]. 31 A. Fatona, J. Moran-Mirabal and M.A. Brook, *Polym. Chem.-UK*, 2019, **10**, 219-227.

[32]. 32 A. Javadi, A. Shockravi, A. Rafieimanesh, A. Malek and S. Ando, *Polym. Int.*, 2015, **64**, 486-495.

[33]. 33 M.A. Olshavsky and H.R. Allcock, *Macromolecules*, 1995, **28**, 6188-6197.

[34]. 34 H.K. Shobha, H. Johnson, M. Sankarapandian, Y.S. Kim, P. Rangarajan, D.G. Baird and J.E. McGrath, *Journal of Polymer Science Part A: Polymer Chemistry*, 2001, **39**, 2904-2910.

[35]. 35 M.A. Olshavsky and H.R. Allcock, *Macromolecules*, 1995, **28**, 6188-6197.

[36]. 36 M. Olshavsky and H.R. Allcock, *Macromolecules*, 1997, **30**, 4179-4183.

[37]. 37 M. Uygun, M.A. Tasdelen and Y. Yagci, *Macromol. Chem. Phys.*, 2010, **211**, 103-110.

[38]. 38 C. Liu, T. Chen, C. Yuan, Y. Chang, G. Chen, B. Zeng, Y. Xu, W. Luo and L. Dai, *RSC Adv.*, 2017, **7**, 46139-46147.